energies

MDPI

Article

Lithium Storage in Nanoporous Complex Oxide $12CaO \cdot 7Al_2O_3$ (C12A7)

Navaratnarajah Kuganathan [1,2,*] and Alexander Chroneos [1,2]

[1] Department of Materials, Imperial College London, London SW7 2AZ, UK; n.kuganathan@imperial.ac.uk (N.K.); alexander.chroneos@imperial.ac.uk (A.C.)
[2] Faculty of Engineering, Environment and Computing, Coventry University, Priory Street, Coventry CV1 5FB, UK; ad0636@coventry.ac.uk (N.K.); ab8104@coventry.ac.uk (A.C.)
* Correspondence: n.kuganathan@imperial.ac.uk; ad0636@coventry.ac.uk

Received: 26 February 2020; Accepted: 22 March 2020; Published: 26 March 2020

Abstract: Porous materials have generated a great deal of interest for use in energy storage technologies, as their architectures have high surface areas due to their porous nature. They are promising candidates for use in many fields such as gas storage, metal storage, gas separation, sensing and magnetism. Novel porous materials which are non-toxic, cheap and have high storage capacities are actively considered for the storage of Li ions in Li-ion batteries. In this study, we employed density functional theory simulations to examine the encapsulation of lithium in both stoichiometric and electride forms of C12A7. This study shows that in both forms of C12A7, Li atoms are thermodynamically stable when compared with isolated gas-phase atoms. Lithium encapsulation through the stoichiometric form ($C12A7:O^{2-}$) turns its insulating nature metallic and introduces Li^+ ions in the lattice. The resulting compound may be of interest as an electrode material for use in Li-ion batteries, as it possesses a metallic character and consists of Li^+ ions. The electride form ($C12A7:e^-$) retains its metallic character upon encapsulation, but the concentration of electrons increases in the lattice along with the formation of Li^+ ions. The promising features of this material can be tested by performing intercalation experiments in order to determine its applicability in Li-ion batteries.

Keywords: C12A7; endoergic; encapsulation; DFT; drone; hazard

1. Introduction

Electrochemical energy storage devices, such as batteries and supercapacitors, have garnered a great deal of attention in the last two decades due to their environmental friendliness, high energy densities and high energy efficiencies. Lithium-ion batteries are the most promising portable power sources with continuous effort being devoted to improving their power densities for use in large-scale applications such as electrical vehicles [1–3] and grid-energy storage systems [4,5]. Furthermore, advanced electronic devices such as drones, unmanned aeroplanes and robots require high-capacity Li-ion batteries [6]. One key area of focus in the development of Li-ion batteries is finding clean, safe, high-energy-density as well as cheap electrode materials. A key challenge in the development of Li-ion batteries has been hazards arising from explosions caused by the destruction of the batteries during electric discharge, heat transfer and several chemical reactions [7]. A variety of electrode materials have been prepared for Li-ion batteries, and their electrochemical activities have been investigated both experimentally [8–11] and theoretically [12–15].

Materials with high porosity and low density are promising candidates for the storage of lithium as they can provide a high surface area for lithium to absorb. Many porous materials [16–18], including metal organic frameworks [19–21] and their derivatives, have been considered as promising electrode materials for Li-ion batteries.

C12A7 is a complex nanoporous oxide consisting of twelve nanocages per unit cell [22–24]. Each cage has an inner space of ~0.4 nm and is interconnected with adjacent cages via a wider opening of ~0.1 nm. This oxide structure is chemically and thermally stable. Furthermore, their constituent metal oxides (Al_2O_3 and CaO) are non-toxic and inexpensive. The stoichiometric form of C12A7 is represented as C12A7:O^{2-}, in which the positively charged framework $[Ca_{24}Al_{28}O_{64}]^{4+}$ is compensated by two O^{2-} ions occupying two cages. In the electride form of C12A7, the framework is compensated by four electrons and its overall composition is denoted by C12A7:e^-. Both forms of C12A7 have been considered for the encapsulation of many metal atoms [25–29] and ions [30–34]. Their surface structures have been investigated as promising catalysts for the activation of small molecules such as CO_2 and N_2 [35–37].

As the bulk nanoporous structure of C12A7 provides a large number of cages (12 per unit cell), this material is of interest for the storage of lithium. A reaction between the insulating C12A7:O^{2-} and Li metal is expected to produce Li^+ ions and electrons in the lattice simultaneously. This experimental recipe can provide an electrode material with Li^+ ions and electron conduction for use in Li-ion batteries.

In this study, we used density functional theory (DFT) with dispersion to study the encapsulation capabilities of Li atoms in both forms of C12A7. This simulation technique enables the calculation of encapsulation energies, the Bader charges of the encapsulated Li atoms, densities of states (DOSs) as well as the charge density plots of resultant complexes. Using this theoretical approach, insights on the applicability of this system as an electrode material can be gained.

2. Computational Methods

The present simulation study was based on DFT calculations [38–40] in order to describe the optimized structures and electronic structures of defect-free, encapsulated and doped C12A7 via the Vienna Ab initio Simulation Program (VASP) code [41–43]. VASP performs fully self-consistent calculations which solve Kohn–Sham (KS) equations within density functional theory. The basic concept underpinning DFT is the use of the electron density, ρ, instead of the wave function. Powerful theorems were provided by Hohenberg and Kohn [40]. They formally established electron density as the central quantity for the purpose of describing electron interactions. With this code, projected augmented wave (PAW) potentials [44] and plane wave basis sets are used. In all calculations, we used a plane wave basis set with a cut-off of 500 eV and 8 *k*-points, generated using a 2 × 2 × 2 Monkhorst–Pack [45] *k*-point mesh. In the modelling of the exchange-correlation energy we used generalized gradient approximation (GGA) as parameterized by Perdew, Burke and Ernzerhof (PBE) [46]. Atomic positions and cell parameters were relaxed using the conjugate gradient algorithm [47]. In all optimized configurations, the amount of force used on the atoms was less than 0.001 eV/Å. Semi-empirical attractive dispersion forces, as described by Grimme et al. [48], were included in all calculations in order to describe the short-range interactions.

Encapsulation energy for a single Li atom in C12A7:e^- was calculated using the following equation:

$$E_{enc} = E_{(Li:C12A7:e^-)} - E_{(C12A7:e^-)} - E_{(Li)} \quad (1)$$

where $E_{(Li:C12A7:e^-)}$ is the total energy of a Li atom encapsulated in C12A7:e^-, $E_{(C12A7:e^-)}$ is the total energy of bulk C12A7:e^- and $E_{(Li)}$ is the energy of an isolated gas-phase Li atom.

Thermodynamically, defect parameters such as formation energies can be defined by the comparison of real (i.e. defective) crystals with isobaric or isochoric ideal (i.e., non-defective) crystals. Models such as the cBΩ [49,50] link the defect formation parameters with thermodynamic relations, as discussed in previous studies [51–53]. The present calculations correspond to the isobaric parameters for the defect processes.

3. Results

3.1. Modelling Bulk C12A7

The stoichiometric C12A7 is cubic (space group $I\bar{4}$ 3d) with a lattice constant of 11.99 Å [20]. Figure 1 shows the relaxed structures of both forms of C12A7. In our previous studies [25,26], we tested the choice of pseudopotentials and basis sets by comparing calculated lattice constants with experimental values. Experimental lattice constants for C12A7:O^{2-} were reported to be a = b = c = 11.99 Å and $\alpha = \beta = \gamma = 90°$ [22]. The calculated values (a = 12.05 Å, b = c = 12.01 Å and $\alpha = 90.02°$, $\beta = 89.95°$ and $\gamma = 89.93°$) are in good agreement with the experimental values. Electronic structures of C12A7:O^{2-} and C12A7:e^- have also been discussed in previous work [25,26] by plotting DOSs. C12A7:O^{2-} is a wide-band-gap insulator. In contrast, C12A7:e^- exhibits a metallic character due to electrons occupying nanocages.

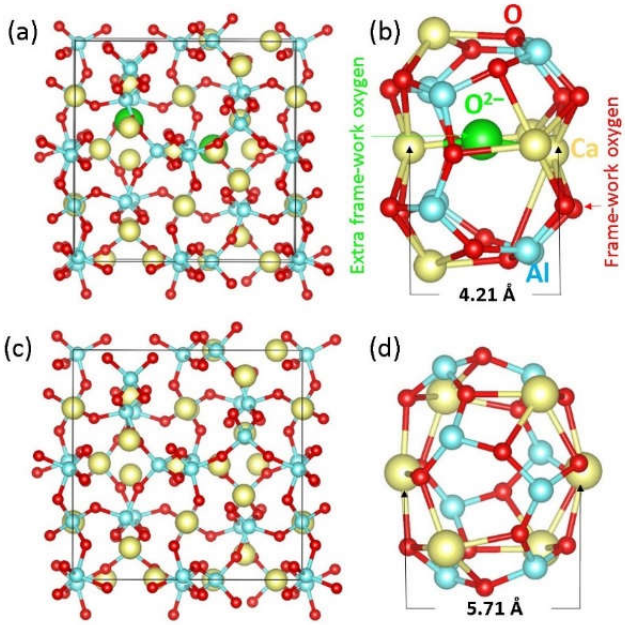

Figure 1. Optimised structures of (**a**) the crystal structure of C12A7:O^{2-}, (**b**) the cage occupying extra-framework O^{2-} ion, (**c**) the crystal structure of C12A7:e^- and (**d**) the cage occupying extra-framework e^-. Cage pole, Ca-Ca distances are calculated to be 4.21 Å and 5.71 Å in C12A7:O^{2-} and C12A7:e^-, respectively.

3.2. Encapsulation of Single Li Atoms in C12A7:O^{2-}

First, we considered the encapsulation of up to four Li atoms added one-by-one in C12A7:O^{2-}. Figure 2 shows the optimised structures of Li atoms occupying cages in C12A7:O^{2-}. In all cases, Li atoms bind to the cage wall oxygen atoms to form Li-O bonds. The Li-O bond distances ranged from between 1.83 and 1.97 Å (Table 1). The encapsulation energy of a second Li into the pre-existing single Li in C12A7:O^{2-} was calculated using the following equation:

$$E_{enc} = E_{(2Li:C12A7:O^{2-})} - E_{(Li:C12A7:O^{2-})} - E_{(Li)} \quad (2)$$

where $E_{(2Li:C12A7:O^{2-})}$ is the total energy of two Li atoms encapsulated in C12A7:O^{2-}, $E_{(Li:C12A7:O^{2-})}$ is the total energy of a single Li atom encapsulated in C12A7:O^{2-} and $E_{(Li)}$ is the energy of an isolated gas-phase Li atom. Exoergic encapsulation energy is calculated for all cases, implying that the Li atoms are more stable inside the cages of C12A7:O^{2-} than in their isolated form. Consequent encapsulation energies do not increase with the number of Li atoms. This could be due to the different pre-encapsulated host structures in the consequent encapsulation of Li. Bader charge analysis [54] shows that Li atoms lose their outer electrons to form Li^+ ions which are then attracted by cage wall O^{2-} ions. The magnetic moment of C12A7:O^{2-} is zero. Encapsulation introduces electrons (~one per Li) in the lattice, making the resultant compounds magnetic. The magnetic moment increases with the addition of Li (refer to Table 1). This is due to an increase in the amount of electrons upon further

addition of Li. Ca-Ca cage pole distance, which is an indication of distortion of the lattice, slightly increases with the addition of Li. This is further confirmed by the small increase seen in the volume with respect to the volume of C12A7:O^{2-}.

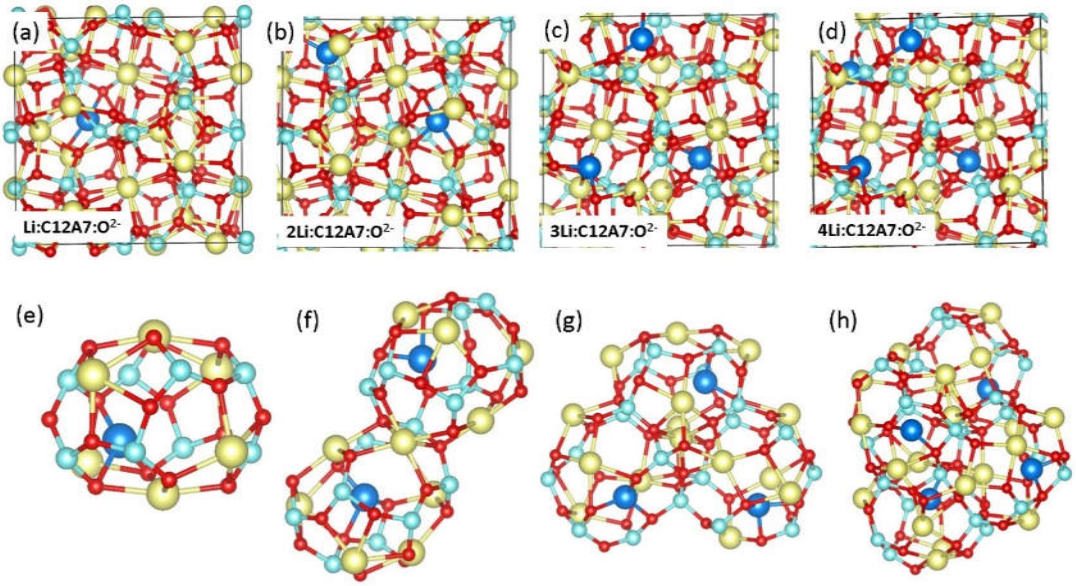

Figure 2. (**a**–**d**) Relaxed structures of Li:C12A7:O^{2-}, 2Li:C12A7:O^{2-}, 3Li:C12A7:O^{2-} and 4Li:C12A7:O^{2-} and (**e**–**h**) corresponding relaxed cages occupying Li atoms.

The calculated total DOS shows that C12A7:O^{2-} is an insulator, as discussed in previous work [25,26] (refer to Figure 3a). Peaks correspond with the extra-framework O^{2-} ions which are observed between 2.00 and 3.00 eV (Figure 3f) and the charge density associated with these peaks is shown in Figure 3k. Encapsulation of the first Li shifts the Fermi level towards the conduction band and the system becomes metallic (Figure 3b). This is due to the electron released from encapsulated Li. This is further confirmed by the atomic DOS of Li (Figure 3g) as well as the electron charge density plot showing the electron occupying a cage. Further encapsulation does not alter the Fermi energy a great deal. However, the electron density increases near the Fermi level (Figure 3 (c–e)). This is also confirmed by their atomic DOSs. Electron charge density increases with the addition of Li, as explained previously (Figure 3 (l–o)).

The simulation results in this section reveal that the encapsulation of Li in C12A7:O^{2-} can change its insulating behaviour to metallic and introduce Li^{+} ions in the lattice simultaneously. The resulting material could be of interest as an electrode material for Li-ion batteries.

Table 1. Encapsulation energies, Bader charges on the encapsulated Li atoms, magnetic moments of the encapsulated complexes, Ca-Ca cage pole distances, Li-O bond distances and volume changes due to the encapsulation. Total Bader charges are shown in parentheses.

System	Encapsulation Energy (eV)	Bader Charges on Li (|e|)	Magnetic Moment (μ)	Cage Pole Ca-Ca Separation (Å)	Li-O Bond Distances (Å)	Volume Change (%)
Li.C12A7:O^{2-}	–1.93 eV	+1.00 (+1.00)	0.85	5.62	1.90–1.93	0.14
2Li.C12A7:O^{2-}	–2.03 eV	+0.66, +0.74 (+1.40)	1.74	5.63–5.67	1.83–1.97	0.24

3Li.C12A7:O^2_-	–1.09 eV	+0.64, +0.74, +0.53 (+1.91)	2.67	5.66–5.70	1.84–1.97	0.32
4Li.C12A7:O^2_-	–0.85 eV	+0.74, +0.69, +0.51, +0.50 (+2.44)	3.56	5.67–5.80	1.88–1.97	0.61

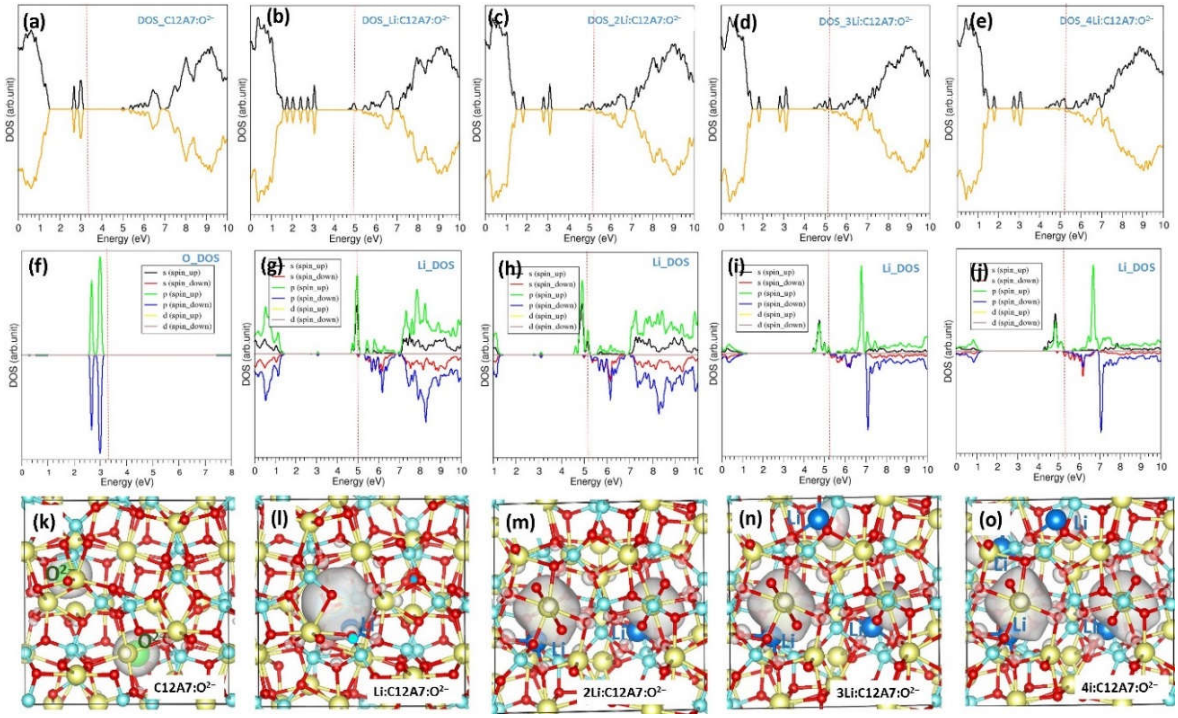

Figure 3. (**a–e**) Total densities of states (DOSs) of C12A7:O^{2-}, Li.C12A7:O^{2-}, 2Li.C12A7:O^{2-}, 3Li.C12A7:O^{2-} and 4Li.C12A7:O^{2-}. (**f–j**) Corresponding atomic DOSs and (**k–o**) corresponding charge density plots associated with extra-framework O^{2-} in C12A7:O^{2-} and electrons introduced by the Li encapsulation. Black and orange parts of the total DOSs (a–e) correspond to spin-up and spin-down states. Red vertical lines correspond to the Fermi energy level.

3.3. Encapsulation of Single Li Atoms in C12A7:e^-

Next, we considered the encapsulation of single Li atoms (up to four) in the empty cages of C12A7:e^-.Figure 4 shows the optimised structures together with the cages occupied by Li atoms. Li atoms are located in the centre of the cages for the first two Li encapsulations. Further substitution leads to slightly different complexes, in which Li forms bonds with cage wall O^{2-} ions. Encapsulation energies appear as negative, meaning that Li atoms prefer to encapsulate within the cages of C12A7:e^- (Table 2). For the third and fourth Li atoms, the encapsulation becomes strong. This may be due to the attractive interaction between Li^+ ions and O^{2-} ions. Bader charge analysis shows that Li^+ ions are present in the first two Li atoms. Further encapsulation reduces the charge transfer of Li. C12A7:e^- is non-magnetic. Encapsulation of the first two Li atoms does not change the magnetic behaviour. In the case of the third and fourth Li atoms, the resulting complexes exhibit magnetic behaviour. This could be due to the incomplete charge transfer of Li in these complexes. There was a very small change in the Ca-Ca cage pole distances in all cases, meaning that distortion due to the encapsulation is small. This is further confirmed by the small volume changes.

The calculated DOS shows that C12A7:e^- is metallic (Figure 5 a). Consequent encapsulation increases the concentration of electrons in the lattice, with this being further confirmed by the increase in electronic states near the Fermi level (Figure 5 (b–e)) . The Fermi energy does not change significantly upon encapsulation. The atomic DOSs of Li atoms for all configurations are shown in Figure 4 (f–i). Charge density plots associated with the extra-framework electrons are shown in Figure

5 (j–n). In C12A7:e⁻, four electrons are uniformly distributed. Upon encapsulation, the electron density in the lattice increases due to the additional electrons coming from the Li atoms.

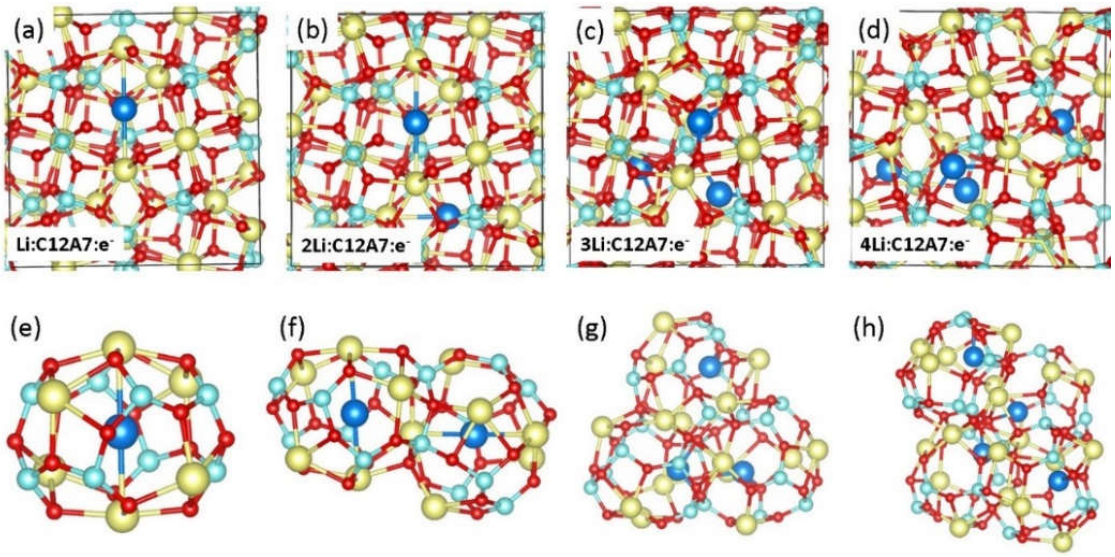

Figure 4. (**a–d**) Relaxed structures of Li.C12A7:e⁻, 2Li.C12A7:e⁻, 3Li.C12A7:e⁻ and 4Li.C12A7:e⁻ and (**e–h**) the corresponding relaxed cages occupying Li atoms.

Table 2. Encapsulation energies, Bader charges on the encapsulated Li atoms, magnetic moments of the encapsulated complexes, Ca-Ca cage pole distances, Li-O bond distances and volume changes due to the encapsulation. The total Bader charges are shown in parentheses.

System	Encapsulation Energy (eV)	Bader Charges on Li (|e|)	Magnetic Moment (μ)	Cage Pole Ca-Ca Separation (Å)	Li-O Bond Distances (Å)	Volume Change (%)
Li.C12A7:e⁻	–0.87 eV	+1.00 (+1.00)	0.00	5.88–5.90	--	0.21
2Li.C12A7:e⁻	–0.65 eV	+1.00, +1.00 (+2.00)	0.00	5.89–5.92	--	0.49
3Li.C12A7:e⁻	–1.83 eV	+0.51, +0.44, +0.48 (+1.43)	1.80	5.62–5.71	1.95–1.99	0.48
4Li.C12A7:e⁻	–1.02 eV	+0.51, +0.17, +0.33, +0.33 (+1.34)	0.47	5.66–5.69	1.94–1.98	0.66

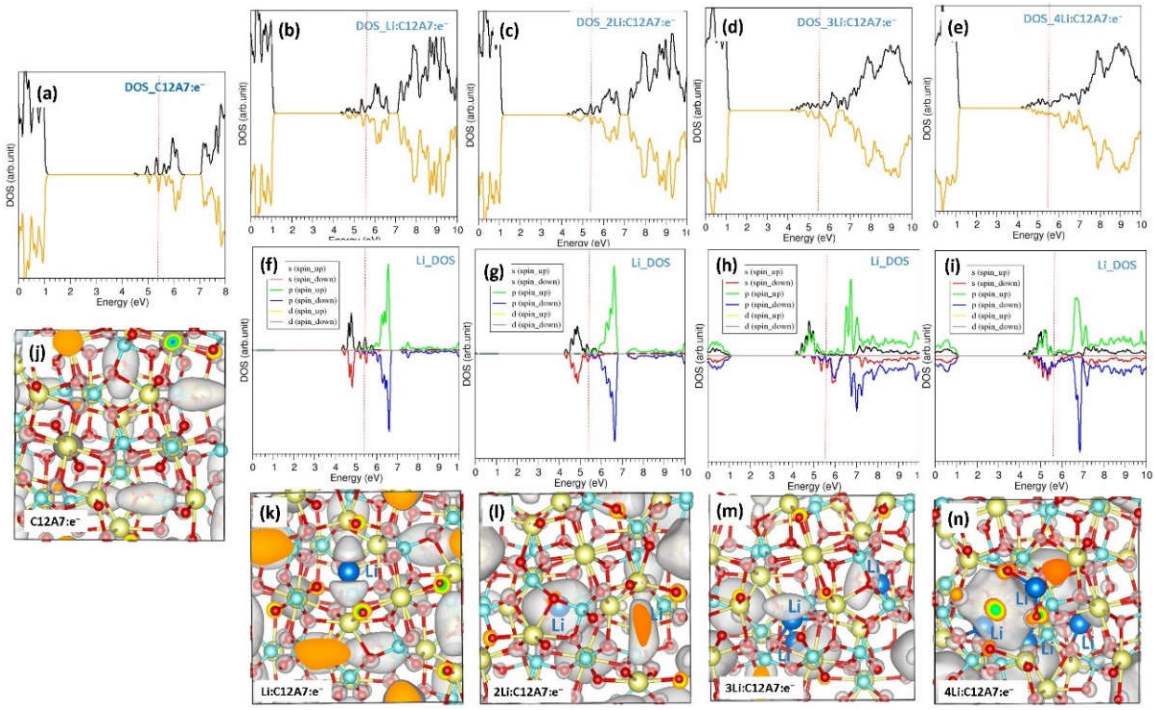

Figure 5. (**a**–**e**) Total DOSs of C12A7:e⁻, Li.C12A7:e⁻, 2Li.C12A7:e⁻, 3Li.C12A7:e⁻ and 4Li.C12A7:e⁻, (**f**–**i**) corresponding atomic DOSs and (**j**–**n**) corresponding charge density plots associated with extra-framework e⁻ in C12A7:e⁻ and electrons introduced by the Li encapsulation. The black and orange parts of the total DOSs (a–e) correspond to spin-up and spin-down states. Red vertical lines correspond to the Fermi energy level.

4. Conclusions

Porous materials provide a high surface area to trap a large volume of Li atoms. The capacity and efficiency of a material depends upon the nature of the porosity having a large number of cages to encapsulate Li atoms. DFT simulations were applied to examine the encapsulation capability of C12A7 for use in Li-ion batteries. Both forms of C12A7 encapsulate Li atoms exothermically, suggesting that Li atoms are more stable than their isolated forms. Bader analysis shows that a Li atom loses approximately one electron and that the resultant Li^+ ion becomes attracted by cage wall O^{2-} ions. The insulating behaviour of C12A7:O^{2-} turns metallic upon encapsulation, leaving the resultant complex Li^+ rich. Thus, it is promising for use as an electrode material in Li-ion batteries. The electride form (C12A7:e⁻) also produces Li^+ ions upon encapsulation, retaining its metallic character together with an increased electron concentration. Furthermore, the resultant composites formed by Li and C12A7:O^{2-} are magnetic. In the case of electride forms, however, only when there is a high content of Li encapsulation is magnetic behaviour exhibited. To conclude, we have shown that Li storage in C12A7 merits consideration by the community and that experimental work is required to investigate this system in view of battery applications.

Author Contributions: Computation N.K.; Writing, N.K.; Analysis and Editing, N.K., A.C. All authors have read and agreed to the published version of the manuscript.

Funding: This research was financially supported by the European Union's H2020 Programme under Grant Agreement no 824072–HARVESTORE.

Acknowledgments: We acknowledge Coventry University and the Imperial College London for providing computing facilities.

Conflicts of Interest: The authors declare no conflict of interest

References

1. Whittingham, M.S. Lithium Batteries and Cathode Materials. *Chem. Rev.* **2004**, *104*, 4271–4302.
2. Goodenough, J.B.; Kim, Y. Challenges for Rechargeable Li Batteries. *Chem. Mater.* **2010**, *22*, 587–603.
3. Tarascon, J.M.; Armand, M. Issues and challenges facing rechargeable lithium batteries. *Nature* **2001**, *414*, 359–367.
4. Bruce, P.G.; Freunberger, S.A.; Hardwick, L.J.; Tarascon, J.-M. Li–O_2 and Li–S batteries with high energy storage. *Nat. Mater.* **2011**, *11*, 19–29.
5. Mauger, A.; Julien, C.M. Critical review on lithium-ion batteries: Are they safe? Sustainable? *Ionics* **2017**, *23*, 1933–1947.
6. Yoo, H.D.; Markevich, E.; Salitra, G.; Sharon, D.; Aurbach, D. On the challenge of developing advanced technologies for electrochemical energy storage and conversion. *Mater. Today* **2014**, *17*, 110–121.
7. Quintiere, J.G. On methods to measure the energetics of a lithium ion battery in thermal runaway. *Fire Saf. J.* **2020**, *111*, 102911.
8. Li, M.; Lu, J.; Chen, Z.; Amine, K. 30 Years of Lithium-Ion Batteries. *Adv. Mater.* **2018**, *30*, 1800561.
9. Padhi, A.K.; Nanjundaswamy, K.S.; Goodenough, J.B. Phospho-olivines as Positive-Electrode Materials for Rechargeable Lithium Batteries. *J. Electrochem. Soc.* **1997**, *144*, 1188–1194.
10. Nishimura, S.-i.; Hayase, S.; Kanno, R.; Yashima, M.; Nakayama, N.; Yamada, A. Structure of Li_2FeSiO_4. *J. Am. Chem. Soc.* **2008**, *130*, 13212–13213.
11. Masquelier, C.; Croguennec, L. Polyanionic (Phosphates, Silicates, Sulfates) Frameworks as Electrode Materials for Rechargeable Li (or Na) Batteries. *Chem. Rev.* **2013**, *113*, 6552–6591.
12. Armstrong, A.R.; Kuganathan, N.; Islam, M.S.; Bruce, P.G. Structure and Lithium Transport Pathways in Li_2FeSiO_4 Cathodes for Lithium Batteries. *J. Am. Chem. Soc.* **2011**, *133*, 13031–13035.
13. Clark, J.M.; Barpanda, P.; Yamada, A.; Islam, M.S. Sodium-ion battery cathodes $Na_2FeP_2O_7$ and $Na_2MnP_2O_7$: Diffusion behaviour for high rate performance. *J. Mater. Chem. A* **2014**, *2*, 11807–11812.
14. Jay, E.E.; Rushton, M.J.D.; Chroneos, A.; Grimes, R.W.; Kilner, J.A. Genetics of superionic conductivity in lithium lanthanum titanates. *Phys. Chem. Chem. Phys.* **2015**, *17*, 178–183.
15. Fisher, C.A.J.; Kuganathan, N.; Islam, M.S. Defect chemistry and lithium-ion migration in polymorphs of the cathode material Li_2MnSiO_4. *J. Mater. Chem. A* **2013**, *1*, 4207–4214.
16. Liu, Z.; Yuan, X.; Zhang, S.; Wang, J.; Huang, Q.; Yu, N.; Zhu, Y.; Fu, L.; Wang, F.; Chen, Y.; et al. Three-dimensional ordered porous electrode materials for electrochemical energy storage. *NPG Asia Mater.* **2019**, *11*, 1–21.
17. Li, Y.; Fu, Z.-Y.; Su, B.-L. Hierarchically Structured Porous Materials for Energy Conversion and Storage. *Adv. Funct. Mater.* **2012**, *22*, 4634–4667.
18. Shobana, M.K.; Kim, Y. Improved electrode materials for Li-ion batteries using microscale and sub-micrometer scale porous materials—A review. *J. Alloy Compd.* **2017**, *729*, 463–474.
19. Xu, G.; Nie, P.; Dou, H.; Ding, B.; Li, L.; Zhang, X. Exploring metal organic frameworks for energy storage in batteries and supercapacitors. *Mater. Today* **2017**, *20*, 191–209.
20. Xie, X.-C.; Huang, K.-J.; Wu, X. Metal–organic framework derived hollow materials for electrochemical energy storage. *J. Mater. Chem. A* **2018**, *6*, 6754–6771.
21. Ke, F.-S.; Wu, Y.-S.; Deng, H. Metal-organic frameworks for lithium ion batteries and supercapacitors. *J. Solid State Chem.* **2015**, *223*, 109–121.
22. Imlach, J.A.; Dent Glasser, L.S.; Glasser, F.P. Excess oxygen and the stability of "$12CaO.7A_{12}O_3$". *Cem. Concr. Res.* **1971**, *1*, 57–61.
23. Watauchi, S.; Tanaka, I.; Hayashi, K.; Hirano, M.; Hosono, H. Crystal growth of $Ca_{12}A_{l1}4O_{33}$ by the floating zone method. *J. Cryst. Growth* **2002**, *237*, 801–805.
24. Kim, S.W.; Matsuishi, S.; Nomura, T.; Kubota, Y.; Takata, M.; Hayashi, K.; Kamiya, T.; Hirano, M.; Hosono, H. Metallic State in a Lime—Alumina Compound with Nanoporous Structure. *Nano Lett.* **2007**, *7*, 1138–1143.
25. Kuganathan, N.; Gkanas, E.; Chroneos, A. Encapsulation and substitution of Fe in C12A7 ($12CaO{\cdot}7Al_2O_3$). *AIP Adv.* **2020**, *10*, 015242.
26. Kuganathan, N.; Chroneos, A.; Grimes, R.W. The encapsulation selectivity for anionic fission products imparted by an electride. *Sci. Rep.* **2019**, *9*, 1–11.
27. Kuganathan, N.; Chroneos, A. Technetium Encapsulation by A Nanoporous Complex Oxide $12CaO{\cdot}7Al_2O_3$ (C12A7). *Nanomaterials* **2019**, *9*, 816.
28. Kuganathan, N.; Grimes, R.W.; Chroneos, A. Encapsulation of heavy metals by a nanoporous complex oxide $12CaO \cdot 7Al_2O_3$. *J. Appl. Phys.* **2019**, *125*, 165103.
29. Nurse, R.W.; Welch, J.H.; Majumdar, A.J. The $12CaO{\cdot}7Al_2O_3$ Phase in the CaO-Al_2O_3 System. *Trans. J. Br. Ceram. Soc.* **1965**, *64*, 323–332.

30. Hayashi, F.; Tomota, Y.; Kitano, M.; Toda, Y.; Yokoyama, T.; Hosono, H. NH2– Dianion Entrapped in a Nanoporous 12CaO·7Al_2O_3 Crystal by Ammonothermal Treatment: Reaction Pathways, Dynamics, and Chemical Stability. *J. Am. Chem. Soc.* **2014**, *136*, 11698–11706.
31. Hayashi, K.; Hirano, M.; Hosono, H. Thermodynamics and Kinetics of Hydroxide Ion Formation in 12CaO·7Al_2O_3. *J. Phys. Chem. B* **2005**, *109*, 11900–11906.
32. Jeevaratnam, J.; Glasser, F.P.; Glasser, L.S.D. Anion Substitution and Structure of 12CaO·7A1_2O_3. *J. Am. Ceram. Soc.* **1964**, *47*, 105–106.
33. Zhmoidin, G.I.; Chatterjee, A.K. Conditions and mechanism of interconvertibility of compounds 12CaO.7Al_2O_3 and 5CaO.3Al_2O_3. *Cem. Concr. Res.* **1984**, *14*, 386–396.
34. Miyakawa, M.; Kamioka, H.; Hirano, M.; Kamiya, T.; Sushko, P.V.; Shluger, A.L.; Matsunami, N.; Hosono, H. Photoluminescence from Au ion-implanted nanoporous single-crystal 12CaO·7Al_2O_3. *Phys. Rev. B* **2006**, *73*, 205108.
35. Toda, Y.; Hirayama, H.; Kuganathan, N.; Torrisi, A.; Sushko, P.V.; Hosono, H. Activation and splitting of carbon dioxide on the surface of an inorganic electride material. *Nat. Commun.* **2013**, *4*, 1–8.
36. Kitano, M.; Kanbara, S.; Inoue, Y.; Kuganathan, N.; Sushko, P.V.; Yokoyama, T.; Hara, M.; Hosono, H. Electride support boosts nitrogen dissociation over ruthenium catalyst and shifts the bottleneck in ammonia synthesis. *Nat. Commun.* **2015**, *6*, 1–9.
37. Kuganathan, N.; Hosono, H.; Shluger, A.L.; Sushko, P.V. Enhanced N2 Dissociation on Ru-Loaded Inorganic Electride. *J. Am. Chem. Soc.* **2014**, *136*, 2216–2219.
38. Kohn, W. Overview of Density Functional Theory. In *Density Functional Theory*; Gross, E.K.U., Dreizler, R.M., Eds.; Springer: Boston, MA, USA, 1995; pp. 3–10.
39. Kohn, W.; Sham, L.J. Self-Consistent Equations Including Exchange and Correlation Effects. *Phys. Rev.* **1965**, *140*, A1133.
40. Hohenberg, P.; Kohn, W. Inhomogeneous Electron Gas. *Phys. Rev.* **1964**, *136*, B864–B871.
41. Kresse, G.; Furthmüller, J. Efficient iterative schemes for ab initio total-energy calculations using a plane-wave basis set. *Phys. Rev. B* **1996**, *54*, 11169–11186.
42. Kresse, G.; Joubert, D. From ultrasoft pseudopotentials to the projector augmented-wave method. *Phys. Rev. B* **1999**, *59*, 1758–1775.
43. Vasp manual: https://www.vasp.at/documentation/ (23.01.2020).
44. Blöchl, P.E. Projector augmented-wave method. *Phys. Rev. B* **1994**, *50*, 17953–17979.
45. Monkhorst, H.J.; Pack, J.D. Special points for Brillouin-zone integrations. *Phys. Rev. B* **1976**, *13*, 5188–5192.
46. Perdew, J.P.; Burke, K.; Ernzerhof, M. Generalized Gradient Approximation Made Simple. *Phys. Rev. Lett.* **1996**, *77*, 3865–3868.
47. Press, W.H.; Teukolsky, S.A.; Vetterling, W.T.; Flannery, B.P. *Numerical Recipes in C: The Art of Scientific Computing*, 2nd ed.; Cambridge University Press:Cambridge, UK; 1992; p. 994.
48. Grimme, S.; Antony, J.; Ehrlich, S.; Krieg, H. A consistent and accurate ab initio parametrization of density functional dispersion correction (DFT-D) for the 94 elements H-Pu. *J. Chem. Phys.* **2010**, *132*, 154104.
49. Varotsos, P. Defect volumes and the equation of state in α-PbF2. *Phys. Rev. B* **2007**, *76*, 092106.
50. Varotsos, P. Comparison of models that interconnect point defect parameters in solids with bulk properties. *J. Appl. Phys.* **2007**, *101*, 123503.
51. Chroneos, A.; Vovk, R.V. Modeling self-diffusion in UO_2 and ThO_2 by connecting point defect parameters with bulk properties. *Solid State Ion.* **2015**, *274*, 1–3.
52. Cooper, M.W.D.; Grimes, R.W.; Fitzpatrick, M.E.; Chroneos, A. Modeling oxygen self-diffusion in UO_2 under pressure. *Solid State Ion.* **2015**, *282*, 26–30.
53. Chroneos, A. Connecting point defect parameters with bulk properties to describe diffusion in solids. *Appl. Phys. Rev.* **2016**, *3*, 041304.
54. Bader, R.F.W. The zero-flux surface and the topological and quantum definitions of an atom in a molecule. *Theor. Chem. Acc.* **2001**, *105*, 276–283.